NASA TECHNICAL NOTE

NASA TN D-7017

HYPERVELOCITY PARTICLE ACCELERATOR EVALUATION

by R. S. Marriott and T. P. Sciacca, Jr.

Goddard Space Flight Center
Greenbelt, Md. 20771

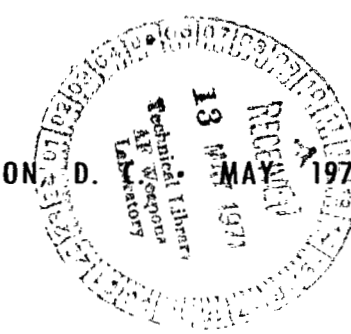

NATIONAL AERONAUTICS AND SPACE ADMINISTRATION • WASHINGTON, D. C. • MAY 1971

1. Report No. NASA TN D-7017	2. Government Accession No.	3. Recipient's Catalog No.
4. Title and Subtitle Hypervelocity Particle Accelerator Evaluation		5. Report Date May 1971 6. Performing Organization Code
7. Author(s) R. S. Marriott and T. P. Sciacca, Jr.		8. Performing Organization Report No.
9. Performing Organization Name and Address Goddard Space Flight Center Greenbelt, Maryland 20771		10. Work Unit No. G-997 11. Contract or Grant No.
12. Sponsoring Agency Name and Address National Aeronautics and Space Administration Washington, D.C. 20546		13. Type of Report and Period Covered Technical Note 14. Sponsoring Agency Code

15. Supplementary Notes

This report is a republication of NASA-Goddard Space Flight Center Document X-735-69-518, November 1969.

16. Abstract

This document contains an evaluation of a hypervelocity impact facility claiming a projectile velocity of 20 to 25 km/s. Solar-cell test panels, subjected to bombardment in the accelerator chamber to determine the change in power output after exposure to hypervelocity impacts and cryogenic conditions, were selected for the experiment. This document describes the experimental procedure and results.

17. Key Words Suggested by Author Micrometeoroids Accelerators	18. Distribution Statement Unclassified—Unlimited		
19. Security Classif. (of this report) Unclassified	20. Security Classif. (of this page) Unclassified	21. No. of Pages 19	22. Price* $3.00

*For sale by the National Technical Information Service, Springfield, Virginia 22151

CONTENTS

HYPERVELOCITY PARTICLE ACCELERATOR EVALUATION*

by
R. S. Marriott
and
T. P. Sciacca, Jr.
Goddard Space Flight Center

INTRODUCTION

The primary objective of this investigation was to locate an accelerator capable of firing simulated micrometeoroid particles at velocities of 20 to 25 km/s under the following constraints:

(1) The projectile mass should be fixed, and the accelerator should be able to fire 10^{-6}-g projectiles.

(2) Each firing should result in multiple impacts on the specified target.

A request for information on such an accelerator prompted only one reply—from Rhodes and Bloxsom, Canoga Park, California. An evaluation was undertaken to obtain preliminary data on micrometeoroid impact on solar cells for missions through the asteroid belt and to ascertain the usefulness of a hypervelocity impact facility for future studies. This document contains an evaluation of the tests conducted at the contractor's facility.

PROJECTILE ACCELERATOR

The projectile accelerator (Figure 1) uses an electrical arc discharge to heat hydrogen gas in a closed chamber to a temperature of 30,000° K and a pressure of 25,000 psi. A tungsten electrode in the hydrogen chamber receives power from a capacitor bank with a storage capacity of 15,000 joules. A conical expansion nozzle is attached to the exit port of the hydrogen chamber. A Mylar diaphragm is used to seal the exit port. The projectiles are attached to the Mylar diaphragm with scotch tape on the hydrogen chamber side of the diaphragm. The specimens are mounted perpendicular to the axis of the expansion nozzle at a distance of approximately 6 ft.

The entire apparatus is enclosed in a vacuum chamber, and fittings were made to cool the specimens to the cryogenic temperature selected for the experiment, −135°C. The 1- by 5-ft viewing ports

*This report is a republication of NASA-Goddard Space Flight Center Document X-735-69-518, November 1969.

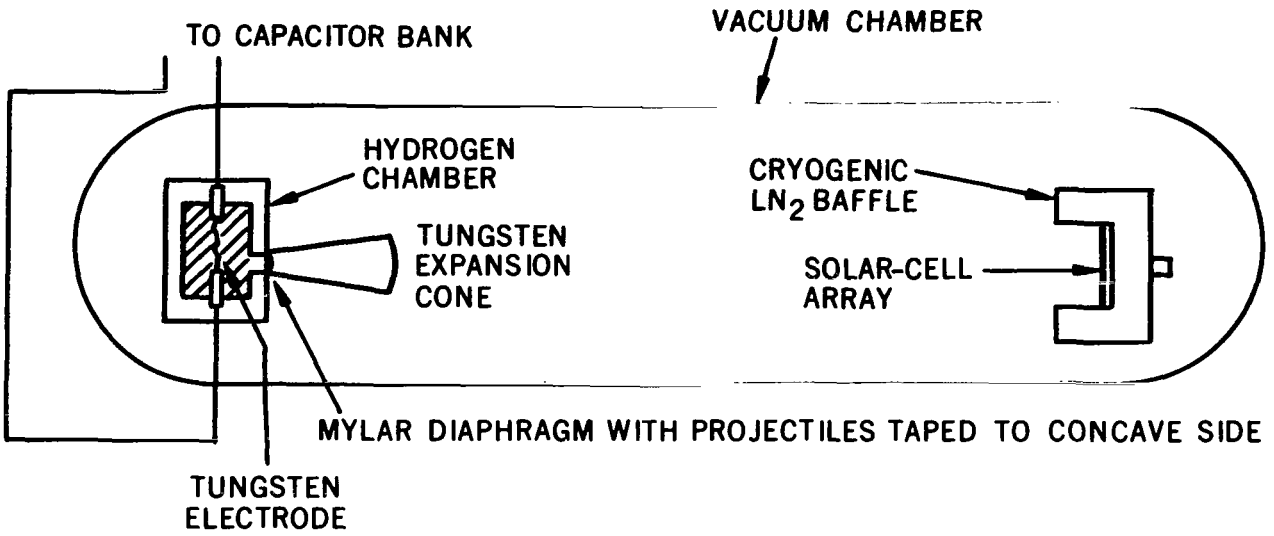

Figure 1—Accelerator schematic diagram.

on both sides of the vacuum chamber (not shown in Figure 1) permit the use of photodetectors and a camera for velocity determination.

The fact that only one contractor responded to the request for services simplified the evaluation. The main objective was to determine maximum projectile velocity. The contractor proposed measuring projectile velocity with a smear camera, and verifying the measurement by calculating the P/d* values from craters made by the projectiles in 2219-T37 aluminum. The agreement stated that a P/d value of 2.65 for the projection of glass spheres into 2219-T37 aluminum corresponds to a velocity of 25 km/s. While this relationship was being verified, it was disclosed that the P/d values used by the contractor came from a curve obtained from smear camera data, and not from an existing formula for P/d.

However, several formulas do exist for deriving P/d. They are the result of both experimental and theoretical studies. In one of Bjork's papers on hypervelocity impact (Reference 1) he states the following formula for depth of penetration P when aluminum targets and aluminum projectiles are used:

$$P = 1.09(mv)^{1/3}, \tag{1}$$

where

P = depth of penetration (cm),

m = projectile mass (g),

and

v = projectile velocity (km/s).

*The ratio P/d is a nondimensional crater parameter, which relates the depth of penetration P of a projectile into a target to the diameter d of the projectile. Investigators used this ratio to characterize projectile velocity.

For an aluminum projectile with a mass of 10^{-6} g and a velocity of 25 km/s, Equation 1* gives a value of $P = 3.18 \times 10^{-2}$ cm. A spherical aluminum projectile of 10^{-6}-g mass and 2.7-g/cm^3 density gives a particle diameter of 89 μm, or 8.9×10^{-3} cm, and from this, a P/d of 3.57. This formulation is for the projection of aluminum spheres into aluminum targets. Investigators (Reference 2) have stated that penetration is an exponential function of the ratio of projectile and target densities:

$$P \sim \left(\frac{\rho_p}{\rho_t}\right)^n , \tag{2}$$

where

P = depth of penetration,

ρ_p = projectile density,

ρ_t = target density,

and

$0 < n < 1$.

Because the densities of glass and aluminum are fairly close (2.5 g/cm^3 and 2.7 g/cm^3, respectively), the ratio $(\rho_p/\rho_t)^n$ is fairly insensitive to the choice of exponent n. Denardo** suggests the use of $n = 0.425$. Combining Equation 2 with the equation developed by Denardo and others (Reference 3) for hard-aluminum targets, we find that

$$P/d = 3.121 \times 10^{-3} d^{1/18} v^{2/3} \tag{3}$$

yields

$$P/d = 3.121 \times 10^{-3} d^{1/18} v^{2/3} \left(\frac{\rho_p}{\rho_t}\right)^{0.425} , \tag{4}$$

where

P/d = dimensionless ratio relating depth of penetration to projectile diameter,

d = projectile diameter (ft),

v = projectile velocity (ft/s),

ρ_p = projectile density (g/cm^3),

and

ρ_t = target density (g/cm^3).

For a glass sphere of 10^{-6}-g mass at 25 km/s, Equation 4 yields a value of $P/d = 3.62$.

Because the contractor contended that the foregoing formulation did not apply to glass projectiles and aluminum targets, particles consisting of both glass and aluminum spheres were used for one

*This formula is of particular interest because the contractor claims that it agrees with his experimental data.
**Personal communication.

of the test runs. It was believed that the resultant crater distribution would be useful in the derivation of projectile velocity and would also clarify the validity of the foregoing equations for the glass projectile, aluminum target configuration.

As previously mentioned, the contractor used a smear camera to determine projectile velocity. The limitations of this technique are described under test results.

An attempt was then made to develop an optical-sensing system capable of determining projectile velocity (Figure 2). Two photomultiplier tubes were placed adjacent to one of the viewing ports of the accelerator chamber. Narrow-bandpass filters were placed between the photomultiplier assembly and the viewing port. The outputs of the photomultiplier were fed to a dual-beam oscilloscope. The filters were selected to permit passage of a spectral wavelength characteristic of silicon. Oscilloscope observations gave the flight time of the glass projectiles over the fixed distance between the two photomultiplier tubes; from the flight time the velocity was derived. (Lack of time and available equipment greatly hampered the development of this apparatus.)

SOLAR CELLS

Bowman and others (Reference 4) investigated solar-cell performance after hypervelocity impact at much lower velocities (2.65 km/s). Fager (Reference 5) reported on solar cells subjected to comparable velocities.* Fager reports certain conclusions which appear to oppose the accepted theory of hypervelocity impact. For example, he states in his concluding remarks that penetration is not affected by an increase in projectile velocity in the 60,000- to 90,000-ft/s range (i.e., 18.3 km/s to 27.4 km/s). Therefore, the reason for selecting solar-cell panels as test specimens was twofold: to obtain data on solar-cell degradation on impact by hypervelocity projectiles at 25 km/s and to clarify certain aspects of Fager's test results.

SELECTION OF PROJECTILE FLUX

Before the test was conducted, it was necessary to select the size and quantity of projectiles to be fired at the solar-cell test panels. It was decided to conduct two tests: one with 10^{-6}-g mass projectiles (Figure 3), and one with 10^{-8}-g mass projectiles. The contractor claimed that he could fire a mix of projectiles having a preselected mass distribution. Although variable mass is an important characteristic of all micrometeoroid flux models, in this test an uncontrolled mass distribution would have made it impossible to determine the mass of the projectile causing specific solar-cell damage.

Kessler's detailed report** describes the meteoroid environment to be expected in the course of a Jupiter flyby mission. Assuming the conditions of the Kessler model for a 600-day flight, we have

$$\frac{N_a}{A} \approx m^{-0.84}, \quad 10^{-9} \leqslant m \leqslant 10^{-2} \tag{6}$$

*Rhodes and Bloxsom performed the experimental work.

**Kessler, D., "The Interplanetary Meteoroid Environment," Manned Spacecraft Center unpublished manuscript, April 1969.

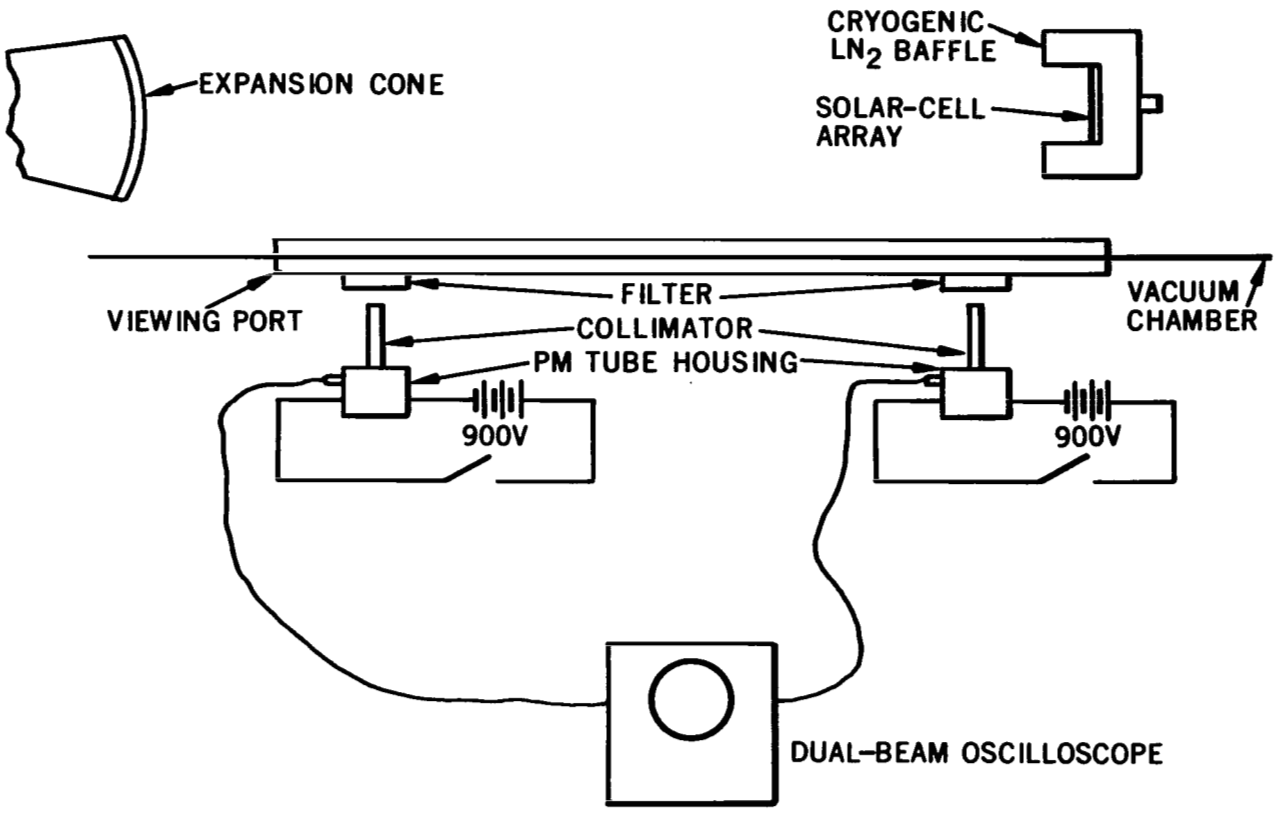

Figure 2—Photomultiplier device schematic.

and

$$\frac{N_c}{A} \approx m^{-1.207}, \quad 10^{-6} \leqslant m \leqslant 10^{0}, \tag{7}$$

where

$\frac{N_a}{A}$ = the number of asteroidal impacts per unit area,

$\frac{N_c}{A}$ = the number of cometary impacts per unit area,

and

m = micrometeoroid mass (g).

Equations 6 and 7 represent a nominal-flux model; therefore, the values obtained should be adjusted to give the Kessler maximum-flux model to obtain worse-case results. For cometary impacts, multiply the nominal value by one order of magnitude (i.e., X 10). The maximum asteroidal flux is determined by the relation

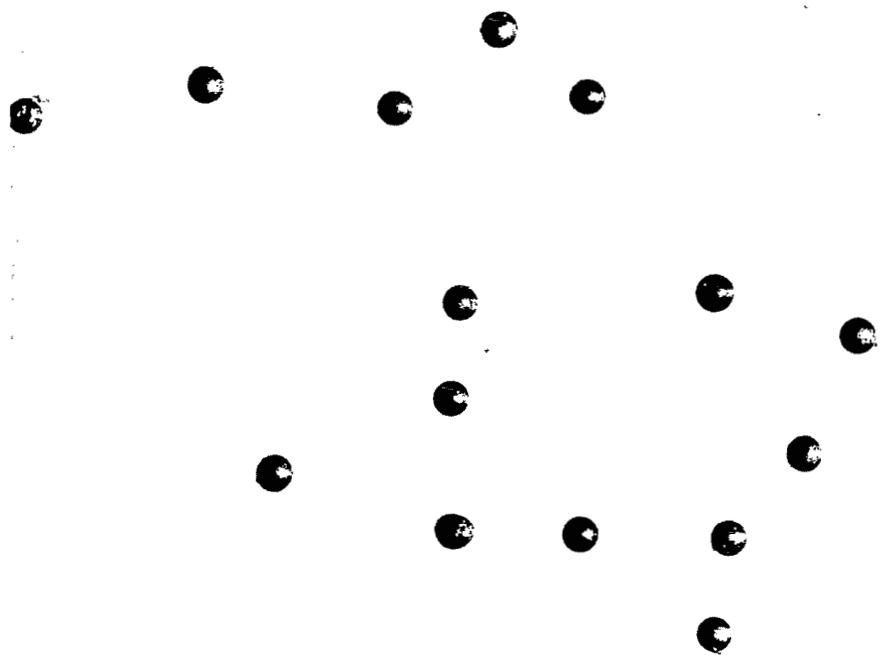

(a) 10^{-6}-g aluminum spheres ($\sim 90\ \mu m$)

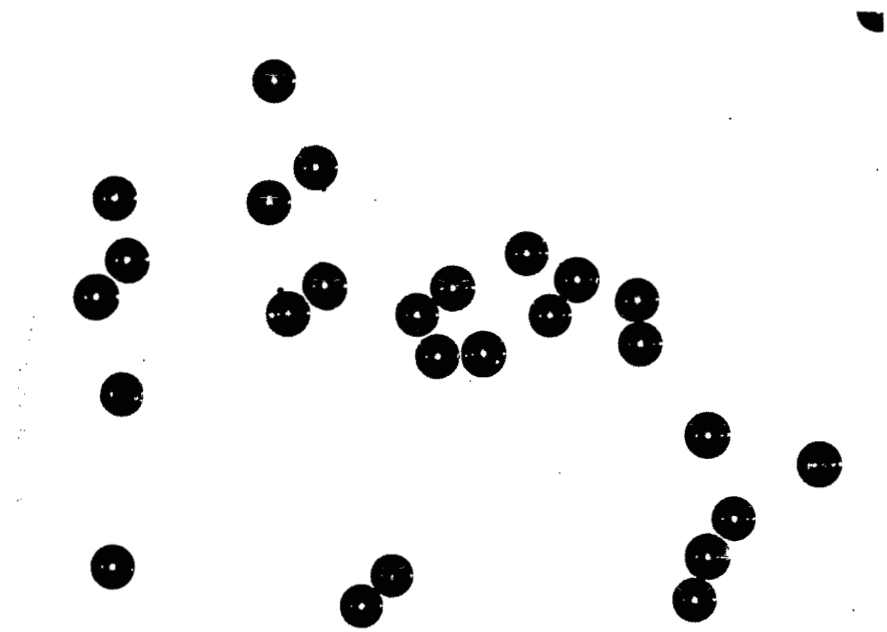

(b) 10^{-6}-g glass spheres ($\sim 110\ \mu m$)

Figure 3—Projectiles used in test run.

$$\frac{N_{a_{max}}}{A} \approx m^{-2/3}, \tag{8}$$

where

$\frac{N_{a_{max}}}{A}$ = maximum number of asteroidal impacts per unit area

and

m = mass of micrometeoroid (g).

Total impacts can be obtained from

$$N_{T_{max}} = \left(\frac{N_{c_{max}}}{A} + \frac{N_{a_{max}}}{A} \right) A', \tag{9}$$

where

$N_{T_{max}}$ = maximum total number of meteoroid impacts,

$\frac{N_{c_{max}}}{A} = \frac{N_c}{A} \times 10$, the maximum number of cometary impacts per unit area,

and

A' = area of solar array.

The area of the solar-cell test panel is approximately 273 cm^2. Applying Equation 9 for a micrometeoroid of mass 10^{-6} g yields $N_T = 3.0$. Because three impacts would not produce enough information to be statistically meaningful, each test panel was subjected to approximately 100 impacts. Table 1 summarizes the test parameters.

Table 1—Test parameters.

Test Parameters	Run 1	Run 2
Projectile type	3:1 glass-to-aluminum ratio	Glass
Projectile mass	10^{-6} g	10^{-8} g
Projectile shape	Spherical	Spherical
Target temperature	−131°C	−123°C
Chamber pressure	35 μm	75 μm
Initial hydrogen pressure	100 psi	100 psi
Final hydrogen pressure	10,000 psi	10,000 psi
Smear camera speed (16-mm frames)	5,000 frames/s	5,000 frames/s

PHOTOMULTIPLIER AND SMEAR CAMERA RESULTS

The photomultiplier technique previously described did not produce reliable data, mainly because of the capacitor bank used for supplying energy to the tungsten electrode. When the capacitor bank discharged to explode the tungsten electrode and initiate acceleration, the field created deflected the oscilloscope trace, causing the initial edge of the upper trace to be lost. A more refined technique (Reference 6), using photomultipliers, should be considered in future testing.

The smear camera technique (Table 2) used by the contractor to obtain projectile velocity involves many uncertainties. The smear camera is positioned so that it can photographically record the progression of the shock front. (The term "shock front" encompasses projectiles, Mylar-diaphragm fragments, gases, and any debris that might be accelerated down the vacuum chamber.) The image appears on the rapidly moving (5000 frames/s) film in the form of a slanted streak (Figure 4), the slope of which is used to calculate the velocity of the shock front. Note that the image on the film is actually a series of streaks of various slopes.

The contractor maintains that the streaks corresponding to solid particles can be distinguished from those caused by gases. Furthermore, he contends that the streaks corresponding to projectiles can be distinguished from those caused by other solid debris if it is assumed that all Mylar-diaphragm fragments and other fragmentary particles are larger than the projectiles and therefore move slower. The investigators take issue with the latter assumption.

Table 2–Contractor's test report.

Projectiles	Velocity (km/s)	
	Obtained by Smear Camera	Calculated from P/d
Glass (Run 1)	21.0	12.5
Aluminum (Run 1)	21.0	19.5
Glass (Run 2)	27.9	26.0

If it can be assumed that the solids and gases can be differentiated on the film, it must also be assumed that vaporization of solids does not occur. However, the exploding Mylar diaphragm produces particle sizes ranging from large irregular fragments to vapor. It is therefore erroneous to assume that all the Mylar particles necessarily travel slower than the projectiles.

The physical dimensions of hypervelocity impact craters can be very useful in the derivation of projectile (impact) velocity.* Before the existing formulas can be applied, the following must be known:

(1) Projectile density.

(2) Target density.

*Impact velocity and projectile velocity will be used interchangeably.

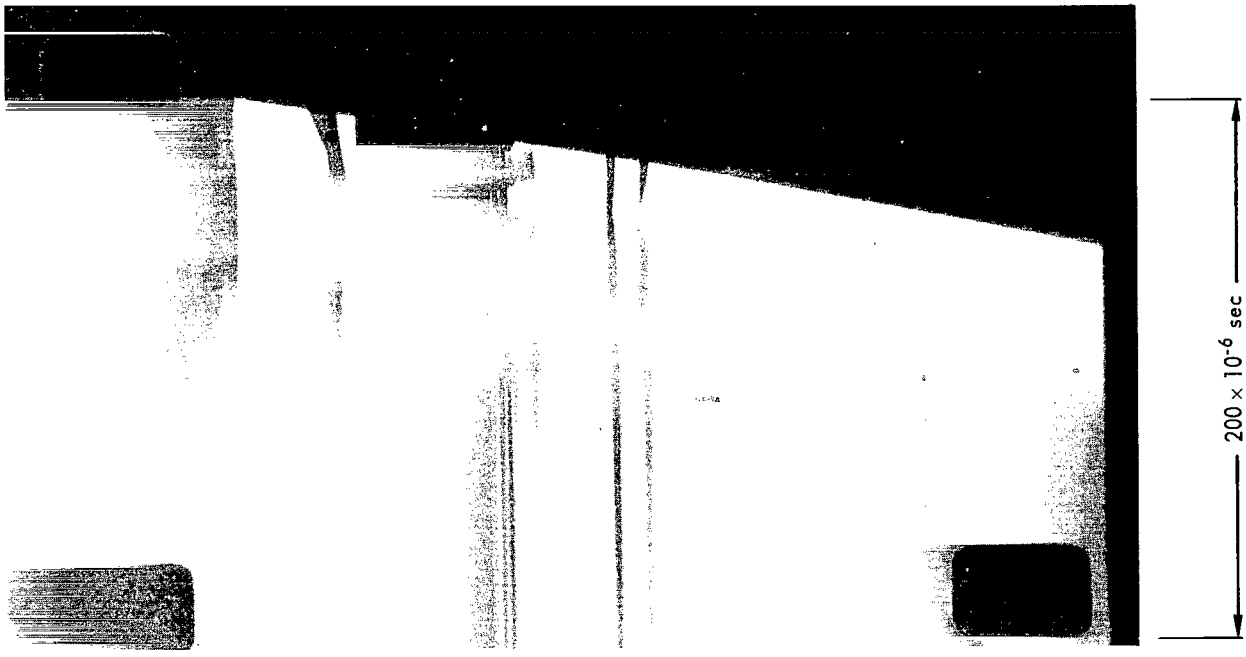

(a) Test run 1

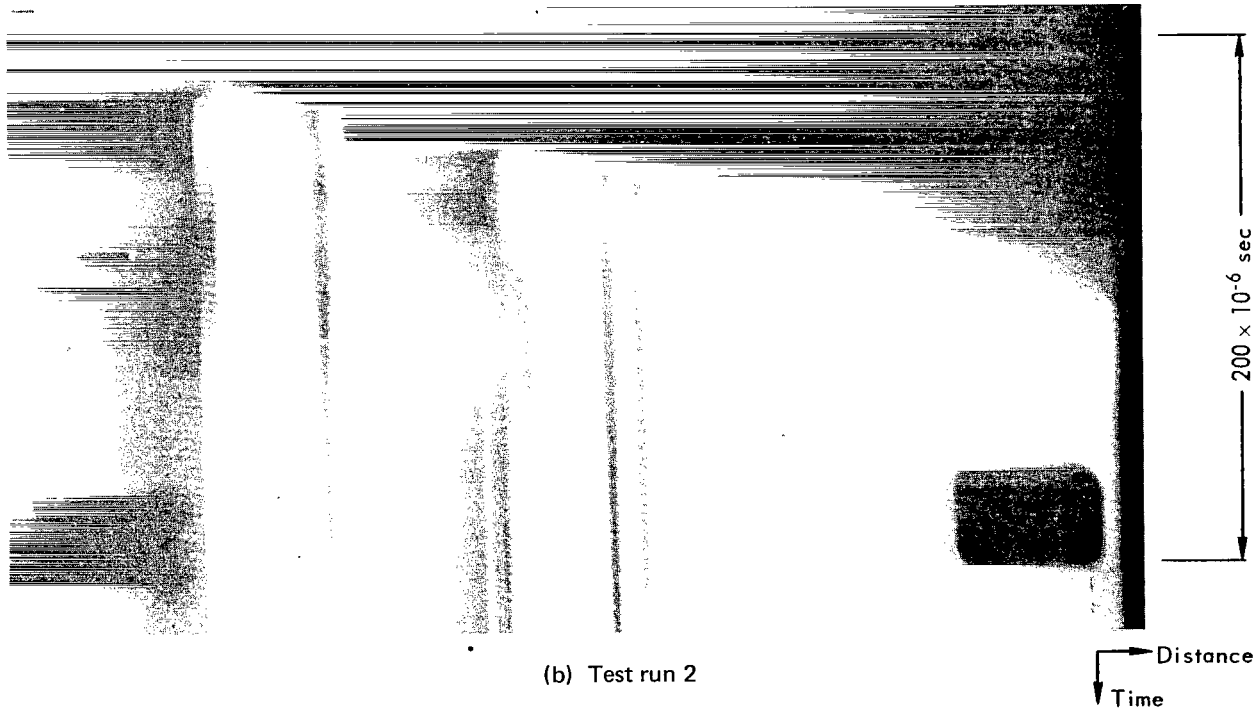

(b) Test run 2

Figure 4—Smear camera photographs.

(3) Projectile mass.

(4) Projectile shape (which need not be precisely known).

Although it appears that these parameters may be easily evaluated, the accelerator contains at least two sources of unwanted projectiles: the Mylar diaphragm and the exploding tungsten electrode. One must therefore determine which craters are made by preselected projectiles and which are caused by "debris."

If the periphery of the crater is not approximately circular, it is assumed that the crater was made by an irregular particle. However, the converse is not true; nonspherical particles can produce nearly circular outlines. Projectiles traveling at hypervelocity speeds vaporize on impact, causing localized vaporization and flow in the target. Therefore, a fairly irregular projectile can make a crater which is difficult to distinguish from a crater caused by a spherical projectile. Also, extremely irregular projectiles (with respect to sphericity) can form sphere-like craters if properly oriented at the time of impact (Reference 7).

Table 3 contains projectile-crater data taken from the aluminum witness plate in the center of the solar-cell test panel. The ratio P/D is another nondimensional crater parameter, which relates the depth of penetration P of a projectile into a target to the diameter D of the crater measured in the plane of the undisturbed surface. Table 3 does not include craters* with noncircular diameters or craters containing any residue. It contains only data from test run 1, which was made with a 3-to-1 glass-sphere-to-aluminum ratio, the mass of the spheres being 10^{-6} g (Figure 4). The craters were characterized by means of a Bausch and Lomb microscope having a vertical adjustment graduated in microns. A 20X objective and a 10X ocular were used for all data recorded.

Crater data on test run 2 were not usable because it was difficult to distinguish between impact craters and surface imperfections in the aluminum witness plate.

To obtain the maximum velocity value, it is necessary to divide the largest value of P in Table 3 by the smallest diameter of the projectiles fired. The aluminum projectiles were 90-μm-diameter spheres, and the glass projectiles were 110-μm-diameter spheres; therefore, using the diameter of the aluminum sphere yields $P/d = 1.58$. This value corresponds to a velocity of 6.6 km/s when Equation 4 is applied. Closer examination of Table 3 reveals that of the 45 craters characterized, 43 can be grouped into three size ranges:

P (depth of penetration)	Number of Craters
26 to 58 μm	22
79 to 98 μm	14
120 to 140 μm	7

This distribution might indicate that the craters resulted from the fragmentation of projectiles. The effective diameter of the impacting projectile would then be smaller and the corresponding P/d

*One crater was omitted from the table which, because of its dimensions (P = 445 μm, D = 1080 μm), is believed to have been caused by debris.

Table 3—Impact crater data.

Penetration Depth, P	Crater Diameter, D	P/D	Penetration Depth, P	Crater Diameter, D	P/D
23.5	63	0.37	79.0	252	0.31
25.5	70	0.36	81.0	273	0.30
26.0	84	0.31	81.5	252	0.32
26.2	95	0.28	82.0	252	0.33
29.3	105	0.28	83.2	231	0.36
29.5	95	0.31	83.5	231	0.36
29.8	105	0.28	84.5	294	0.29
30.1	105	0.29	86.0	294	0.29
30.5	95	0.32	86.5	273	0.32
30.7	105	0.32	87.0	273	0.32
34.3	126	0.27	90.0	294	0.31
39.5	147	0.27	92.0	273	0.34
41.0	147	0.28	93.0	273	0.34
43.5	147	0.30	98.5	315	0.31
46.5	168	0.28	120.5	357	0.34
47.0	168	0.28	124.5	378	0.33
51.0	189	0.27	124.8	378	0.33
52.2	168	0.39	128.0	357	0.36
52.3	178	0.29	137.0	399	0.34
52.4	189	0.28	139.0	420	0.33
57.0	189	0.30	141.0	420	0.34
58.2	178	0.33	141.5	400	0.35
66.0	210	0.31			

value would be larger. However, if fragmentation of projectiles did occur, it would be impossible to determine the P/d values because the resulting diameter of the fragments would be unknown.

In addition, it is improbable that all 45 craters tabulated in Table 3 resulted from fragmented projectiles. (If they did, this facility could not be used when constant projectile mass is required.) To reinforce this premise, the ratio P/D, which is independent of projectile diameter, is given in Table 4. The highest value of P/D is 0.37, and the mean value is 0.32. Alternatively, use the following equation (Reference 3), modified by the density ratio, to calculate P/D:*

$$P/D = 1.403 \times 10^{-1} d^{0.200} v^{0.112} \left(\frac{\rho_p}{\rho_t}\right)^{0.425}, \qquad (10)$$

*Denardo's Equation actually relates P to D_i, the idealized crater diameter, which in all cases is smaller than D.

where

d = diameter of projectile (in.)

and

v = velocity of projectile (ft/s).

For a 110-μm-diameter glass projectile with a velocity of 15 km/s (49,200 ft/s), Equation 10 yields a value of $P/D = 0.40$. However, if $P/D = 0.37$ is substituted in Equation 10 and solved for velocity, the result is 9.7 km/s (31,800 ft/s).

Table 4—Extreme and mean values of depth of penetration P, diameter D, and ratio P/D.

Value	Penetration Depth, P	Crater Diameter, D	P/D
Maximum	141.5	420	0.37
Minimum	23.5	63	0.27
Mean	70.9	222.6	0.32

SOLAR-CELL RESULTS*

Figures 5 through 8 are photographs of solar-cell test panels at the various stages of current-voltage measurement. Figure 6 shows the solar-cell test panels after micrometeoroid exposure, with the aluminum witness plates moved slightly off center to show the overall darkening of the test panel after exposure. This darkening of the test panels caused a decrease in cover-slide transmission. An attempt to clean the test panels before electrical characterization was not entirely successful (Figure 7), and the cover slides were removed. Figure 9 and Table 5 give the results of the electrical testing. Table 6 lists the percent of current loss at various voltages.

Because the test panels were darkened by exposure, it was impossible to determine the percentage of degradation of cover-slide transmission resulting from projectile impacts. Figure 9 shows that most of the damage was confined to the cover glasses. The loss in current caused by the cover glasses and adhesive accounts for the higher curve after glass removal. Current-voltage curves for this solar-cell configuration are typically 4 to 8 percent lower in current with the 6-mil cover slides than without them.

Table 5—Effects of cleaning and glass removal on postexposure open-circuit voltage (V_{oc}).

Measurement	Panel A		Panel B	
	V_{oc} (V)	Degradation (%)	V_{oc} (V)	Degradation (%)
Initial	9.5	—	8.9	—
After exposure	7.2	24	8.4	6
After cleaning	8.4	12	8.2	8
After glass removal	9.0	5	8.3	7

*This section is an abstract of a personal communication from N. Mejia.

Table 6—Effects of cleaning and glass removal on postexposure current at various voltages.

Voltage (V)	Panel A				Panel B			
	Initial Current (mA)	Current Degradation (%)			Initial Current (mA)	Current Degradation (%)		
		After Exposure	After Cleaning	After Glass Removal		After Exposure	After Cleaning	After Glass Removal
0	367	56.4	25.1	-9.0*	375	36.0	32.0	-5.3*
2.0	358	61.5	29.1	-4.7*	365	38.4	35.4	0.0
4.0	345	69.6	37.1	0.0	340	42.6	38.2	2.9
5.0	335	73.7	41.8	6.9	324	45.1	41.4	5.9
6.0	320	83.7	50.0	16.2	300	48.3	45.6	11.7
7.0	288	96.5	60.1	25.7	269	57.2	55.4	25.7

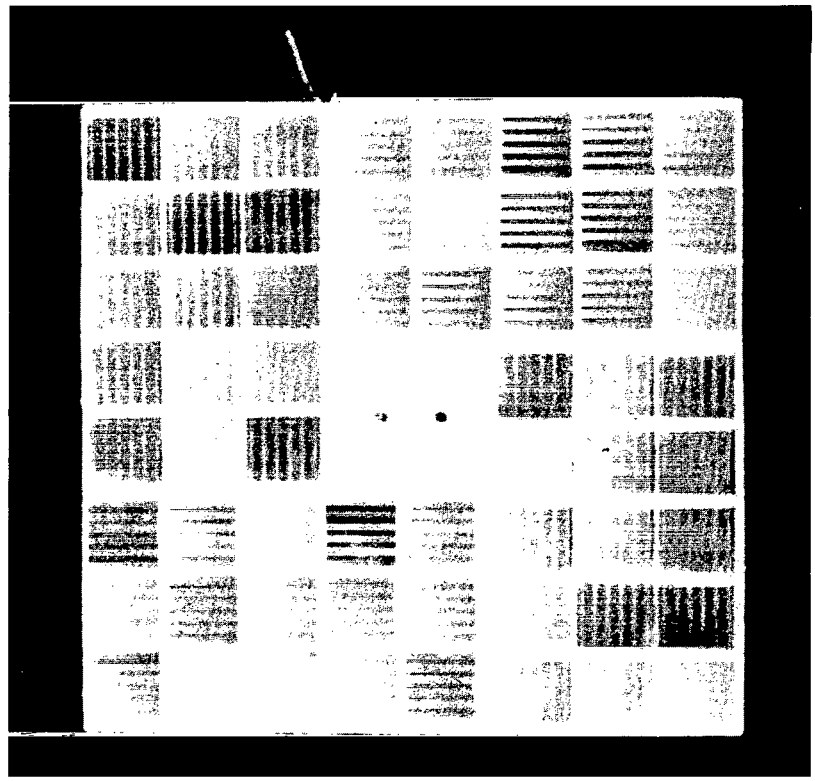

Figure 5—Solar-cell test panel 2 (before exposure).

*Excess current compared to initial panel output results from total elimination of cover-glass and adhesive transmission losses.

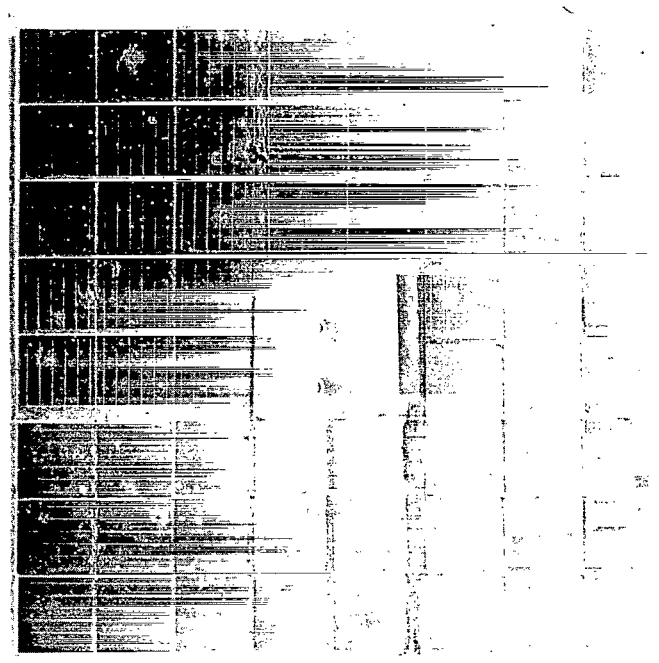

Panel 1

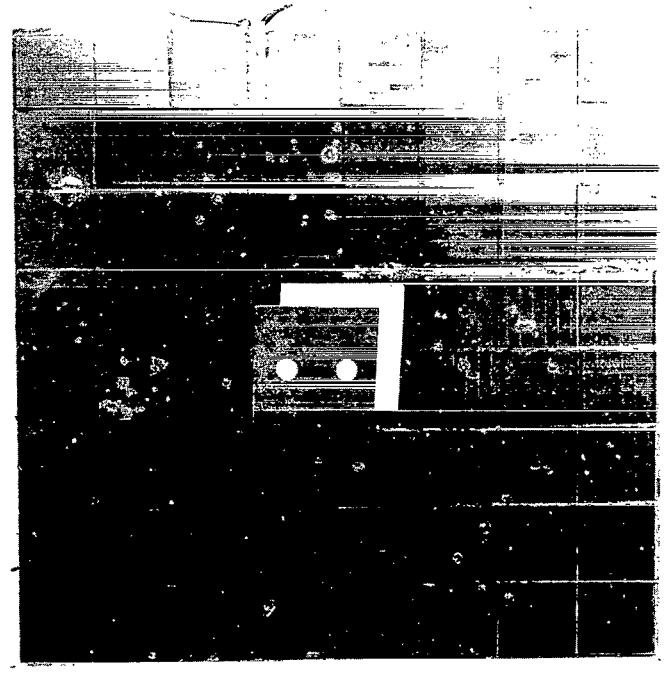

Panel 2

Figure 6—Solar-cell test panels 1 and 2 (after exposure).

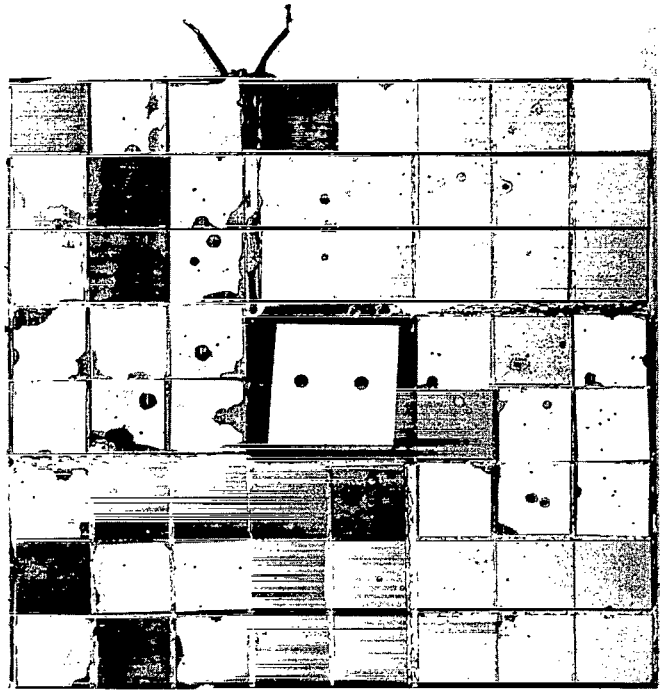

Panel 1

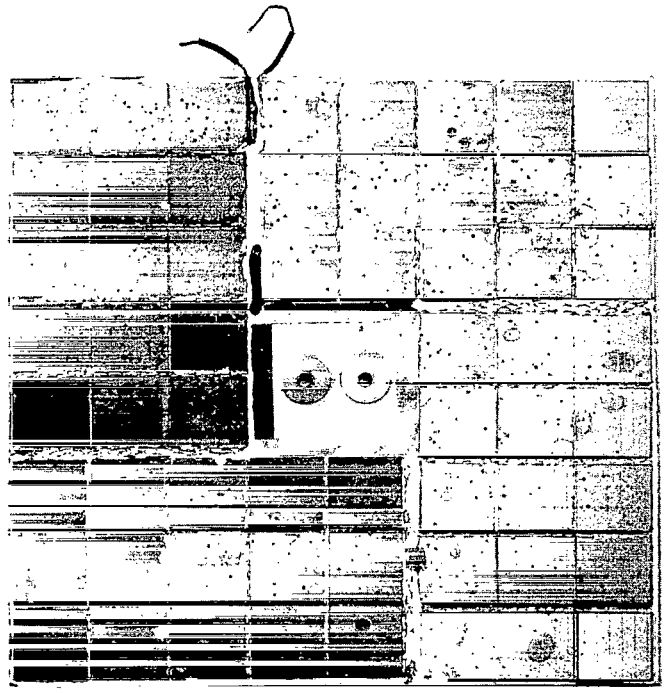

Panel 2

Figure 7—Solar-cell test panels 1 and 2 (after cleaning).

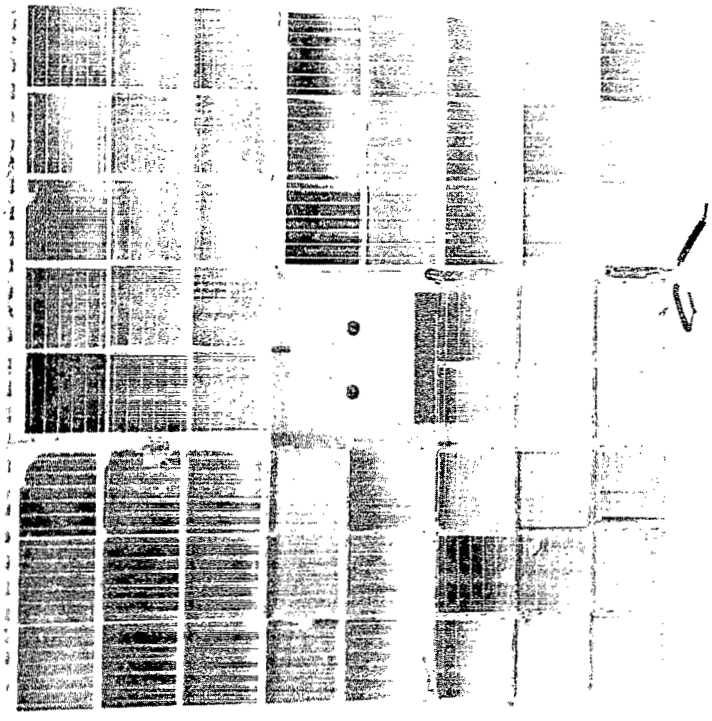

Panel 1

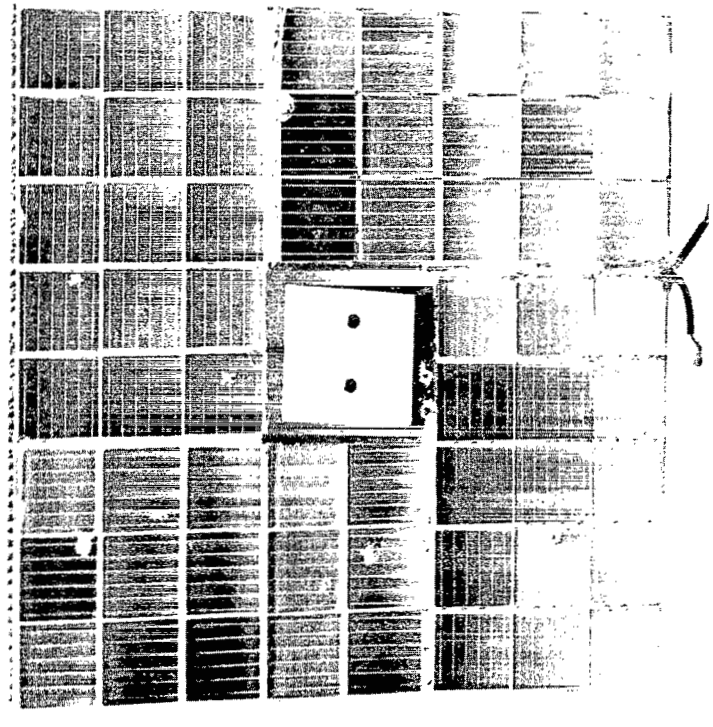

Panel 2

Figure 8—Solar-cell test panels 1 and 2 (after cover-glass removal).

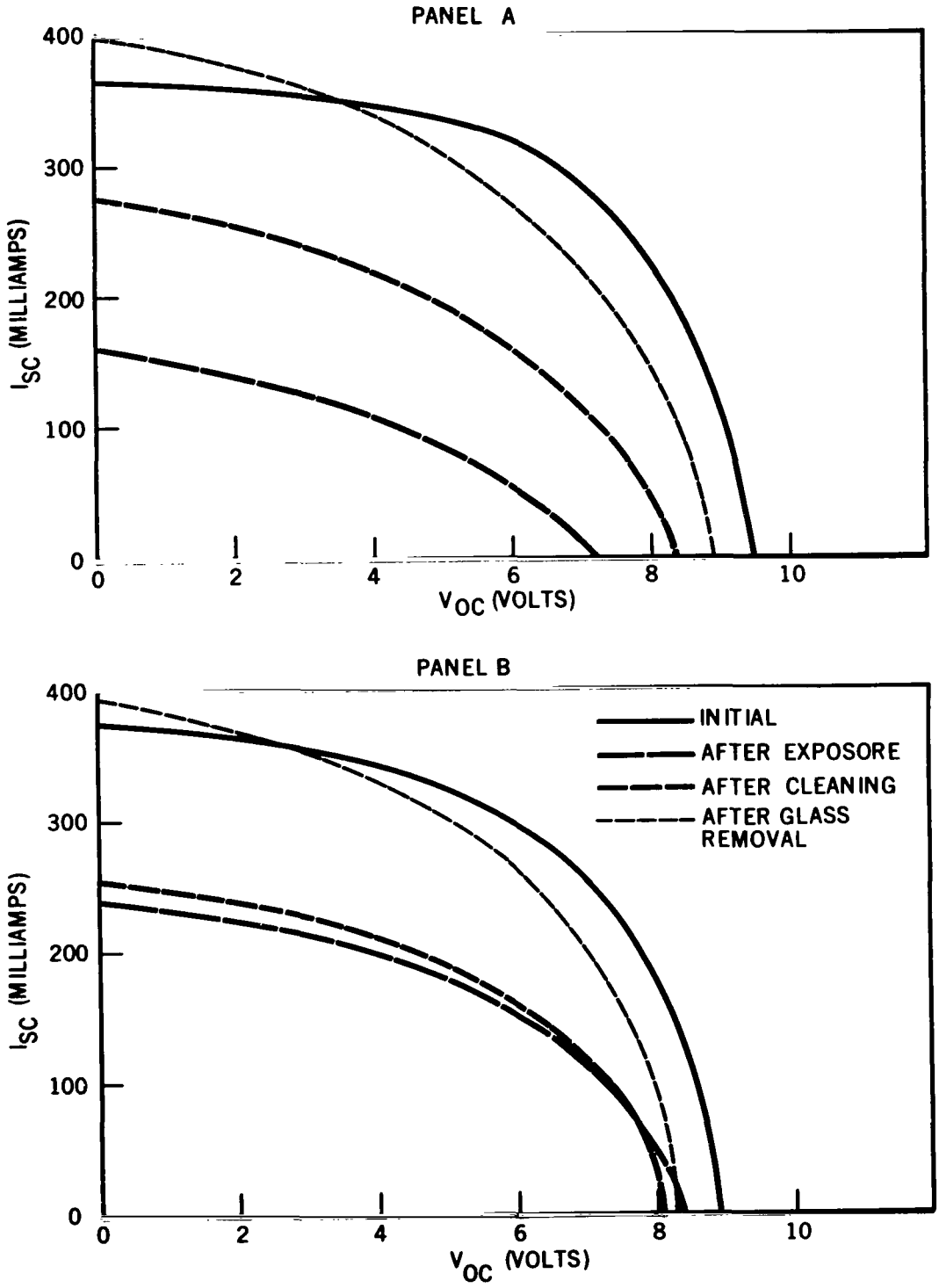

Figure 9—Solar-cell test-panels current-voltage curves at various stages.

CONCLUSIONS

Crater parameters show that projectile velocity in test run 1 did not exceed 10 to 11 km/s. Projectile velocity was not obtained for test run 2, because it was impossible to distinguish craters in the witness plate. The darkening of the test panels during exposure complicated the evaluation of solar-cell damage. The following conclusions have been drawn:

(1) Most of the damage was confined to the cover glasses.

(2) Cracks in solar cells did not always result in failure of the cell; panel 1 had many more cracked cells than panel 2.

(3) Conclusions cannot be drawn from space-flight data because projectile velocity is uncertain and analysis of cover-slide transmission is complicated by darkening of the panels.

The fact that the magnitude of impacts in the tests is much higher than that expected on a flight through the asteroid belt does not exclude the possibility of using the flight data. For example, if damage to solar-cell arrays at these fluxes is minimal or negligible, the data can be safely extrapolated to lesser fluxes.

RECOMMENDATIONS

In its present state, the facility cannot be used for micrometeoroid simulation except in tests where only relative data is required (e.g., several hull composites tested side by side on the same shot) and projectile velocity is not critical. The facility cannot be used for general micrometeoroid simulation without the following changes:

(1) Determination of projectile velocity by additional instruments that function independently of the smear camera.

(2) Use of a technique for determining projectile integrity during the flight.

(3) Removal from the test run of material responsible for darkening the test specimens.

ACKNOWLEDGMENTS

The authors wish to thank Mr. J. Conn and Mr. M. Balderston, of the Outer Planets Explorer project office, for providing instrumentation support; Mr. Donald Humes, who has had extensive experience with experimental techniques of hypervelocity impact research, for spot-checking and supporting crater data with measurements made at Langley Research Center; Mr. N. Mejia for being responsible for the current-voltage measurements of the solar-cell test panels; and Mr. P. Denardo for advice and suggestions.

Goddard Space Flight Center
National Aeronautics and Space Administration
Greenbelt, Maryland, July 22, 1970
120-34-11-05-51

REFERENCES

1. Bjork, R. L., "Meteroids vs Space Vehicles," *J. Am. Rocket Soc.* 31:803–807, June 1961.

2. Summers, J. L., and Charters, A. C., "High Speed Impact of Metal Projectiles in Targets of Various Materials," *Proc. Third Symposium on Hypervelocity Impact* Armour Research Foundation, Illinois Institute of Technology, Chicago, 1959.

3. Denardo, B. P., Summers, J. L., and Nysmith, C. R., "Projectile Size Effects on Hypervelocity Impact Craters in Aluminum," NASA Technical Note D-4067, National Aeronautics and Space Administration, Washington, D.C., July 1967.

4. Bowman, R. L., Mirtrch, M. J., and Jack, J. R., "Performance of N/P Silicon and Cadmium Sulfide Solar Cells as Affected by Hypervelocity Particle Impact," NASA Technical Note D-5133, National Aeronautics and Space Administration, Washington, D.C., Mar. 1969.

5. Fager, J. A., "Effects of Hypervelocity Impact on Protected Solar Cells," General Dynamics/ Convair Report GDC-CHB-65-011, Convair Division, General Dynamics Corp., San Diego, 1965.

6. Laderman, A. J., Lewis, C. H., and Byron, S. R., "Time-of-Flight Measurement of Particle Velocity," *Astronautics and Aeronautics* 8(3):556–558, Mar. 1969.

7. Denardo, B. P., "Projectile Shape Effects on Hypervelocity Impact Craters in Aluminum," NASA Technical Note D-4953, National Aeronautics and Space Administration, Washington, D.C., Dec. 1968.

NASA-Langley, 1971 —— 11

05U 001 36 51 3DS 71.10 00903
AIR FORCE WEAPONS LABORATORY /WLOL/
KIRTLAND AFB, NEW MEXICO 87117

ATT E. LOU BOWMAN, CHIEF, TECH. LIBRARY

"The aeronautical and space activities of the United States shall be conducted so as to contribute . . . to the expansion of human knowledge of phenomena in the atmosphere and space. The Administration shall provide for the widest practicable and appropriate dissemination of information concerning its activities and the results thereof."

— NATIONAL AERONAUTICS AND SPACE ACT OF 1958

NASA SCIENTIFIC AND TECHNICAL PUBLICATIONS

TECHNICAL REPORTS: Scientific and technical information considered important, complete, and a lasting contribution to existing knowledge.

TECHNICAL NOTES: Information less broad in scope but nevertheless of importance as a contribution to existing knowledge.

TECHNICAL MEMORANDUMS: Information receiving limited distribution because of preliminary data, security classification, or other reasons.

CONTRACTOR REPORTS: Scientific and technical information generated under a NASA contract or grant and considered an important contribution to existing knowledge.

TECHNICAL TRANSLATIONS: Information published in a foreign language considered to merit NASA distribution in English.

SPECIAL PUBLICATIONS: Information derived from or of value to NASA activities. Publications include conference proceedings, monographs, data compilations, handbooks, sourcebooks, and special bibliographies.

TECHNOLOGY UTILIZATION PUBLICATIONS: Information on technology used by NASA that may be of particular interest in commercial and other non-aerospace applications. Publications include Tech Briefs, Technology Utilization Reports and Technology Surveys.

Details on the availability of these publications may be obtained from:

SCIENTIFIC AND TECHNICAL INFORMATION OFFICE

NATIONAL AERONAUTICS AND SPACE ADMINISTRATION

Washington, D.C. 20546